RSC Advances

PAPER

Cite this: *RSC Adv.*, 2019, **9**, 27136

Aminated β-cyclodextrin-grafted Fe_3O_4-loaded gambogic acid magnetic nanoparticles: preparation, characterization, and biological evaluation

Wei Fang,†[a] Ya Ji Dai,†[ab] Ting Wang,[a] Hai Tao Gao,[a] Peng Huang,*[a] Juan Yu,[a] He Ping Huang,[a] Dian Lei Wang *[ac] and Wei Lu Zong[a]

Based on aminated β-cyclodextrin (6-NH_2-β-CD)-grafted Fe_3O_4 and gambogic acid (GA) clathrate complexes, a nanoparticle delivery system was developed with the aim to achieve low irritation, strong targeting, and high bioavailability of a gambogic acid magnetic nanopreparation. 6-NH_2-β-CD grafted onto Fe_3O_4 MNPs was demonstrated by high-resolution transmission electron microscopy, Fourier transform infrared spectroscopy, X-ray diffraction, zeta potential, and magnetic measurements. The average particle size of the Fe_3O_4@NH_2-β-CD MNPs was 147.4 ± 0.28 nm and the PDI was 0.072 ± 0.013. The encapsulation efficiency, drug loading, zeta potential, and magnetic saturation values of the Fe_3O_4@NH_2-β-CD MNPs were 85.71 ± 3.47%, 4.63 ± 0.04%, −29.3 ± 0.42 mV, and 46.68 emu g^{-1}, respectively. Compared with free GA, the *in vitro* release profile of GA from Fe_3O_4@NH_2-β-CD MNPs was characterized by two phases: an initial fast release and a delayed-release phase. The Fe_3O_4@NH_2-β-CD MNPs displayed continuously increased cytotoxicity against HL-60 and HepG2 cell lines in 24 h, whereas the carrier Fe_3O_4@NH_2-β-CD MNPs showed almost no cytotoxicity, indicating that the release of GA from the nanoparticles had a sustained profile and Fe_3O_4@NH_2-β-CD MNPs as a tumor tissue-targeted drug delivery system have great potential. Besides, blood vessel irritation tests suggested that the vascular irritation could be reduced by the use of Fe_3O_4@NH_2-β-CD MNPs encapsulation for GA. The $t_{1/2}$ and the AUC of the Fe_3O_4@NH_2-β-CD@GA MNPs were found to be higher than those for the GA solution by approximately 2.71-fold and 2.42-fold in a pharmacokinetic study, respectively. The better biocompatibility and the combined properties of specific targeting and complexation ability with hydrophobic drugs make the Fe_3O_4@NH_2-β-CD MNPs an exciting prospect for the targeted delivery of GA.

Received 1st July 2019
Accepted 30th July 2019

DOI: 10.1039/c9ra04955j

rsc.li/rsc-advances

1. Introduction

Gambogic acid (GA, $C_{38}H_{44}O_8$) is the major active ingredient of gamboge,[1] which has various biological activities, such as antipyretic, analgesic, anti-inflammatory, autophagic, and anti-tumor.[2] Previous studies have shown that GA can activate impaired apoptotic pathways in cancerous cells *via* the down-regulation of telomerase to achieve an anticancer effect.[3] However, the clinical development and applications of GA are limited to date due to its poor water solubility and bioavailability.[4] The use of chemical structure modification methods could solve these problems.[5,6]

Magnetic drug-loaded nanoparticles have become one of the research hotspots in current drug delivery systems due to their non-invasive and high targeting properties.[7] Especially, the immobilization of some molecules onto magnetic nanoparticles has attracted considerable attention, such as macrocyclic host molecules.[8] The aim of such targeted delivery is to load a drug onto highly responsive magnetic nanoparticles, and use the external magnetic field to move and concentrate the nanoparticles on the target organ or the target tissue, thereby increasing the drug concentration and improving the bioavailability of the drug.[9]

Due to their superparamagnetism and biocompatibility, Fe_3O_4 magnetic nanoparticles (Fe_3O_4 MNPs), as magnetic materials, represent an important component,[10] which exhibit many potential applications, including bioseparation, protein adsorption, enzyme immobilization, magnetic resonance imaging, and drug targeting.[11] Fe_3O_4 MNPs have properties of good chemical stability, biocompatibility, and dispensability in various solvents.[12] Many materials, such as noble metals,

[a]The College of Pharmacy, Anhui University of Chinese Medicine, Hefei, 230012, Anhui, China. E-mail: great7701@126.com; dlwang@ahtcm.edu.cn; Fax: +86-0551-68129028; Tel: +86-0551-68129159

[b]Anhui Second People's Hospital, Hefei, 230041, Anhui, China

[c]Anhui Province Key Laboratory of Chinese Medicinal Formula, Hefei, 230012, Anhui, China

† The two authors contributed equally to this work.

surfactants, and polymers, as functional groups have been introduced onto Fe_3O_4 MNPs for new chemical modification, and applications.[13]

β-Cyclodextrin (β-CD) has primary and secondary hydroxyl groups,[14] and has been used as a natural supramolecular host with a cyclic structure, a hydrophilic outer surface and hydrophobic cavity.[15] In the field of chemistry, pharmaceuticals, enzyme mimics, and drug carriers were widespread application[16] where β-CD has potential, as the cavity of β-CD and a small molecule drug could form an inclusive complex, which could enhance the solubility of hydrophobic drugs and reduce undesirable smell and side effects.[17] The cyclodextrins of the host–guest type complexation and their applications in many fields have recently received much attention.[18]

Gambogenic acid (GNA)-loaded folic acid (FA)-armed MNPs (FA-GNA-MNPs) were prepared by our research team, and we confirmed that FA and GNA were successfully conjugated on the Fe_3O_4 core and exhibited substantial inhibitory effects in HeLa cancer cells.[19] Recently, a drug delivery system with the inclusion property of cyclodextrin, the bioadhesive property of GA, and the magnetic property of iron oxide was successfully designed.[18] In this paper, Fe_3O_4@NH_2-β-CD-encapsulated GA magnetic nanoparticles (Fe_3O_4@NH_2-β-CD@GA MNPs) were prepared *via* a co-precipitation method and characterized by high-resolution transmission electron microscopy (HRTEM), Fourier transform infrared spectroscopy (FTIR), vibrating sample magnetometry (VSM), and zeta potential.[20] The study and evaluation of the MNP system's drug-carrying capacity and release performance was carried out by the dialysis method. The hepatocellular carcinoma cell line HepG2 and leukemia HL-60 cell line were used as research objects. The MTT assay was used to explore the anti-tumor effect of the nano drug-loading system on solid tumor cells and non-solid tumor cells. The pathological tissue sections of rabbit ear veins were observed by HE staining to measure the vascular irritancy of the gambogic acid magnetic Fe_3O_4@NH_2-β-CD nanoparticles. The plasma concentration–time curve of GA in rat plasma was measured to evaluate the pharmacokinetic characteristics of the Fe_3O_4@NH_2-β-CD@GA MNPs. It was demonstrated that the water solubility and bioavailability of gambogic acid were improved, and the application scope was expanded. This system can be a promising vehicle for the administration of hydrophobic drugs.

2. Materials and methods

2.1 Chemicals and reagents

Gambogic acid (98%, Sigma-Aldrich, St. Louis, MO, United States); $FeCl_3 \cdot 6H_2O$ (F102739, Shanghai Macklin Biochemical Co., Ltd); $FeCl_2 \cdot 4H_2O$ (RA10220008, BeiJing HengYe ZhongYuan Chemical Co., Ltd); ammonium hydroxide (A801005, Shanghai Macklin Biochemical Co., Ltd); tosyl chloride (T821340, Shanghai Macklin Biochemical Co., Ltd); NaOH, CH_3CN, NaN_3, $(C_6H_5)_3P$, *N*,*N*-dimethylformamide (Shanghai Aladdin Biochemical Technology Co., Ltd); citric acid (C805022, Shanghai Macklin Biochemical Co., Ltd); ethanol (E164502, Shanghai Aladdin Biochemical Technology Co., Ltd); β-cyclodextrin (β-CD, W402826, Shanghai Sinopharm Chemical Reagent Co., Ltd.); methanol (M120521, Shanghai Aladdin Biochemical Technology Co., Ltd.); and phosphoric acid (P816342, Shanghai Aladdin Biochemical Technology Co., Ltd). All reagents were of analytical grade. Water used was deionized water.

2.2 Cells

HepG2 cells, HL-60 cells (China Center for Type Culture Collection); fetal bovine serum (FBS) (GIBCO, No. 16000-044); methyl sulfoxide (US Sigma Corporation, 20170210); dimethyl sulfoxide (US Sigma Corporation, 20170610); thiazolyl blue tetrazolium bromide (MTT, American Sigma Company, lot number MKB06849V); Iscove's modified Dulbecco's medium (IMDM, US HyClone, AB212851); and phosphate-buffered saline (PBS, prepared in our laboratory).

2.3 Animals

All protocols and animal care were authorized by the Animal Care and Use Committee of Anhui University of Chinese Medicine and were in accordance with the Guidelines for the Use of Laboratory Animals. All rats and rabbits were purchased from the Anhui Medical University Experimental Animal Center (Hefei, China). All rats and rabbits were acclimated in an animal breeding room under specific pathogen-free (SPF) conditions (Laboratory License No. SYXK (Wan) 2017-0001). Animal Certificate No. 201800222. Laboratory animal production license No. SCXK (Wan) 2018-0012.

2.4 Synthesis of 6-NH_2-β-CD

β-Cyclodextrin (5.0 g) was dissolved in 40 mL deionized water, and NaOH solution was added dropwise until the solution clarified. Next, *p*-toluenesulfonyl chloride solution containing acetonitrile (0.84 g *p*-TosCl, 3 mL CH_3CN) was added and stirred for 4 h at 10 °C. After the solution was filtered, the filtrate was adjusted to pH 6, and a white precipitate was obtained as 6-OTos-β-CD. 6-OTos-β-CD and NaN_3 were then added to 15 mL ethyl alcohol solution and allowed to undergo a reflux reaction for 15 h. Following distillation, the precipitate was dissolved in 100 mL deionized water and filtered, and the filtrate was added into 100 mL acetone to give a white precipitate, which was washed with acetone/water (v/v = 5 : 1) to give 6-N_3-β-CD. Next, 6-N_3-β-CD and $(C_6H_5)_3P$ were added to 2 mL DMF and stirred for 1 h, then 2 mL $NH_3 \cdot H_2O$ was added and the solution was stirred for 4 h at 20 °C. After the solution was filtered, the filtrate was poured into 80 mL acetone and a white precipitate was obtained as 6-NH_2-β-CD.[21]

2.5 Synthesis of Fe_3O_4@NH_2-β-CD MNPs

$FeCl_3 \cdot 6H_2O$ (2.61 g) and $FeCl_2 \cdot 4H_2O$ (1.05 g) were dissolved in 100 mL deionized water to produce a solution with the concentrations of 0.01 mol L^{-1} and 0.005 mol L^{-1}, respectively. $NH_3 \cdot H_2O$ (W/W: 25%) and citric acid were added at 80 °C until the solution turned dark.[22] Fe_3O_4 MNPs were added into the MES solution. Subsequently, EDCI (191 mg) and NHS (115 mg)

were added and stirred for 1 h. The solution of MES containing 6-NH_2-β-CD (1.1 g) was added and allowed to react for 12 h. The final product was Fe_3O_4@NH_2-β-CD MNPs.[20]

2.6 Preparation of Fe_3O_4@NH_2-β-CD@GA MNPs

The Fe_3O_4@NH_2-β-CD MNPs were prepared using the following procedure: Fe_3O_4@NH_2-β-CD (40 mg) was dissolved in 15 mL PBS at pH 7.4. GA (20 mg) was dissolved in 10 mL methanol. Subsequently, the two solutions were mixed and stirred at room temperature for 48 h. Following centrifugation, the precipitate was lyophilized using a vacuum freeze dryer for 24 h to obtain the Fe_3O_4@NH_2-β-CD@GA MNPs.

2.7 Characterization of the Fe_3O_4@NH_2-β-CD MNPs

FTIR (Thermo Nicolet 6700 ThermoFisher Scientific, USA) spectral analysis of β-CD, 6-OTos-β-CD, 6-N_3-β-CD, 6-NH_2-β-CD, Fe_3O_4@NH_2-β-CD MNPs, and Fe_3O_4@NH_2-β-CD@GA MNPs was performed. X-ray diffraction analysis (XRD, MAC Science MXP18AHF) of the samples (Fe_3O_4 MNPs, Fe_3O_4@NH_2-β-CD MNPs and Fe_3O_4@NH_2-β-CD@GA MNPs) was performed using an X-ray powder diffractometer (Bruker, Germany) equipped with Cu Kα radiation. The physical appearance and nanoparticle size distribution were evaluated using a high-resolution transmission electron microscopy (HRTEM) system (SU8200, Hitachi TEM system; Hitachi High-Technologies Pte Ltd). Solutions of Fe_3O_4@NH_2-β-CD MNPs and Fe_3O_4@NH_2-β-CD@GA MNPs were diluted to optimal concentrations with absolute alcohol and placed on a copper grid prior to the analysis. Hysteresis curves of Fe_3O_4, Fe_3O_4@NH_2-β-CD MNPs and Fe_3O_4@NH_2-β-CD@GA MNPs were determined between −20–20 KOe at 300 K. Determination of the average particle size, polydispersity index (PDI), and zeta potential of Fe_3O_4 MNPs, Fe_3O_4@NH_2-β-CD MNPs, and Fe_3O_4@NH_2-β-CD@GA MNPs were performed using a Malvern particle size analyzer (Zetasizer 3000HS; Malvern Instruments, UK). Each experiment was performed in triplicate ($n = 3$) at 25 °C.

2.8 Drug entrapment efficiency and drug loading

Fe_3O_4@NH_2-β-CD@GA MNPs (10.00 mg) was dissolved in 1 mL methanol, and the unencapsulated GA was separated by ultrasonication for 20 min and supercentrifuged at 12 000 rpm. The concentration of GA in the supernatant was determined by HPLC.[23] The encapsulation efficiency (EE%) and drug loading (DL%) of the Fe_3O_4@NH_2-β-CD@GA MNPs were determined by the following equations:

$$\mathrm{EE\%} = W_E/W_A \times 100\%$$

$$\mathrm{DL\%} = W_E/W_L \times 100\%$$

where W_E is the amount of encapsulated GA in the Fe_3O_4@NH_2-β-CD@GA MNPs, W_A is the amount of GA added in the system, and W_L is the weight of Fe_3O_4@NH_2-β-CD@GA MNPs added in system.

2.9 *In vitro* GA release studies

The *in vitro* release of GA was carried out in PBS (pH 7.4) containing 1% Tween 80. Tween 80 was used to increase the solubility of GA in the buffer solution. The GA solution and Fe_3O_4@NH_2-β-CD@GA MNPs were transferred into a pre-swelled dialysis bag (21 mm, molecular weight cut off 8000–14400 Da, USA), and subsequently, the dialysis bags were sealed and put into 100 mL release medium at 37 ± 0.5 °C and stirred at 100 rpm. At predetermined time intervals, 2 mL dissolution medium was withdrawn and replenished with the same amount of fresh medium. The amount of GA released was analyzed by HPLC.

2.10 Cell viability and proliferation

The *in vitro* cytotoxicity of Fe_3O_4@NH_2-β-CD@GA MNPs against APL HL-60 and HepG2 cells was evaluated using the MTT assay in the following three experimental groups: GA, Fe_3O_4@NH_2-β-CD, and Fe_3O_4@NH_2-β-CD@GA MNPs group.[24,25] The cytotoxicity of HL-60 cells was evaluated across the concentration range of 0.0625, 0.125, 0.250, 0.500, 1.000, 2.000, and 4.000 μg mL^{-1} in triplicate for each group. The cytotoxicity of HepG2 cells was evaluated across the concentration range of 0.094, 0.188, 0.375, 0.750, 1.500, 3.000, and 6.000 μg mL^{-1} in triplicate for each group. Absorbance was measured at 490 nm using a microplate reader (US Bio-Tek, model ELX800MV).

2.11 Vascular irritation

The influence of Fe_3O_4@NH_2-β-CD@GA MNP concentration and ear-vein injection times on vascular irritation in rabbit were tested.[26] Here, 18 white New Zealand rabbits (weighing 2–2.5 kg) were divided randomly into two groups. GA solution (dissolved in normal saline) and Fe_3O_4@NH_2-β-CD@GA MNPs were administered to the right ear vein of the two groups of rabbits at a dose of 4, 8, or 16 mg kg^{-1}, respectively. An equivalent volume of normal saline was administrated as a reference *via* the left ear vein. All the rabbits were treated once daily for 3 days and examined for signs of irritation after administration. The excised tissue samples were fixed in 4% paraformaldehyde, then embedded in paraffin, and subsequently, cut into 5 μm thick paraffin sections and placed on a glass slide. The tissues were stained with hematoxylin and eosin (H&E). The stimulating effect of GA on venous blood vessels after being wrapped with Fe_3O_4@NH_2-β-CD was judged by observing the histopathological changes in the ear veins under a microscope.

2.12 Pharmacokinetic study

Ten SD rats (220 ± 20 g, male) were divided randomly into two groups ($n = 5$) for GA and Fe_3O_4@NH_2-β-CD@GA MNP intravenous administration at a dose of 20 mg kg^{-1}.[27] Blood samples (0.2 mL) were collected from the orbital plexus at specific time intervals (0, 2, 5, 10, 20, 30, 40, 60, 80, 100, 120 min) and put into heparin-containing tubes. Subsequently, the sample was centrifuged at 3000 rpm for 10 min to separate plasma and then stored at −80 °C for further analysis. 10 μL of the internal standard (2 μg mL^{-1} of gambogic acid) was spiked in 100 μL rat

plasma, and subsequently, vortex-mixed with 1 mL ethyl acetate for 10 min. The supernatant was gathered after being centrifuged at 3500 rpm for 10 min and evaporated under nitrogen. Next, 100 μL of methanol was added to the eppendorf tubes to redissolve, and then the solution was centrifuged at 12 000 rpm; 20 μL of the supernatant was analyzed by HPLC.

3. Statistical analysis

All the results are expressed as mean ± standard deviation (SD) and were calculated using GraphPad Prism 7.0. Data were evaluated using the Student's *t*-test. *P* values less than 0.05 were considered to show statistical difference and less than 0.01 was considered to show significant difference.

4. Results and discussion

The synthesis of 6-NH_2-β-CD was achieved by substituting the 6-position hydroxyl group of β-CD with *p*-TosCl, NaN_3, and $P(Ph)_3$ *via* a reduction reaction. Subsequently, the carboxyl group (on the citric acid) on the surface of Fe_3O_4 was activated by EDCI and NHS to react with ammonia on 6-NH_2-β-CD to form an amide, and produced Fe_3O_4@NH_2-β-CD MNPs as the host macromolecule. The GA, which is a highly hydrophobic anti-tumor drug, was the guest component included in the host macromolecule to form the nano complex Fe_3O_4@NH_2-β-CD@GA MNPs (Scheme 1).

4.1 Characterization of the Fe_3O_4@NH_2-β-CD MNPs

The FTIR spectral analysis results of β-CD, 6-NH_2-β-CD, Fe_3O_4@NH_2-β-CD MNPs, and Fe_3O_4@NH_2-β-CD@GA MNPs are shown in Fig. 1. The spectra of the composites are similar to each other because they all contain infrared active bands originating from β-CD. Nonetheless, in the spectral range from 1300 to 1800 cm^{-1} and below 800 cm^{-1}, certain differences can be observed due to the presence of Fe_3O_4.[28] β-CD contains multiple hydroxyl groups, and their reactivity is different. The absorption bands at 3387 cm^{-1} correspond to OH or COOH stretching vibration, and at 1015 and 1135 cm^{-1} are related to the anti-symmetric glycosidic ν_a(C–O–C) vibration and the coupled ν(C–C/C–O) stretching vibration (Fig. 1a-a), respectively, which were, according to the R-1, 4-bond skeleton vibration, and the anti-symmetric vibrations of glycosidic bond (C–O–C).[29] The peaks of 6-NH_2-β-CD at 1635 cm^{-1} are related to the N–H stretching vibration (Fig. 1a-b). The results indicate that –NH_2 was successfully grafted onto the β-CD.[30] The significant peak of Fe_3O_4@NH_2-β-CD was observed at 580 cm^{-1}, which was ascribed to the Fe–O stretching vibration of Fe_3O_4 (Fig. 1a-c). Significant peaks of Fe_3O_4@NH_2-β-CD@GA MNPs at 2950 cm^{-1} observed were due to the C–H bond stretching vibration of citric acid.[31] The absorption peaks at 1637 and 1015 cm^{-1} (Fig. 1a-d)

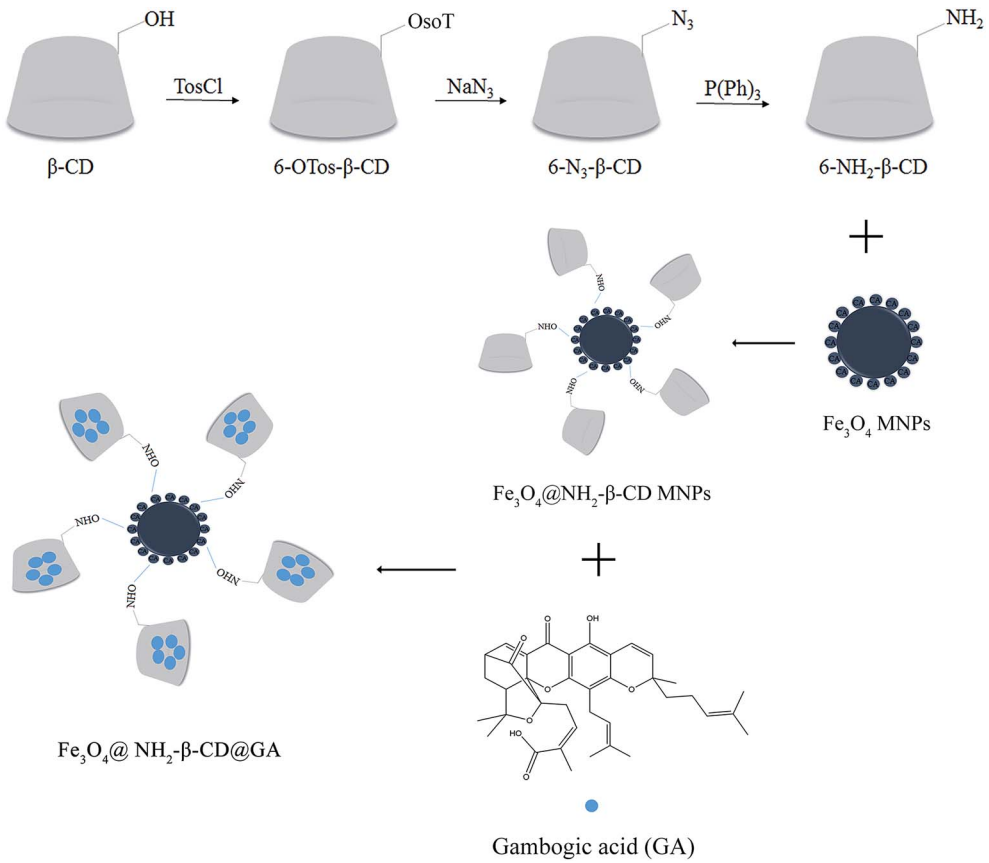

Scheme 1 Schematic diagram of the synthesis process of Fe_3O_4@NH_2-β-CD@GA MNPs.

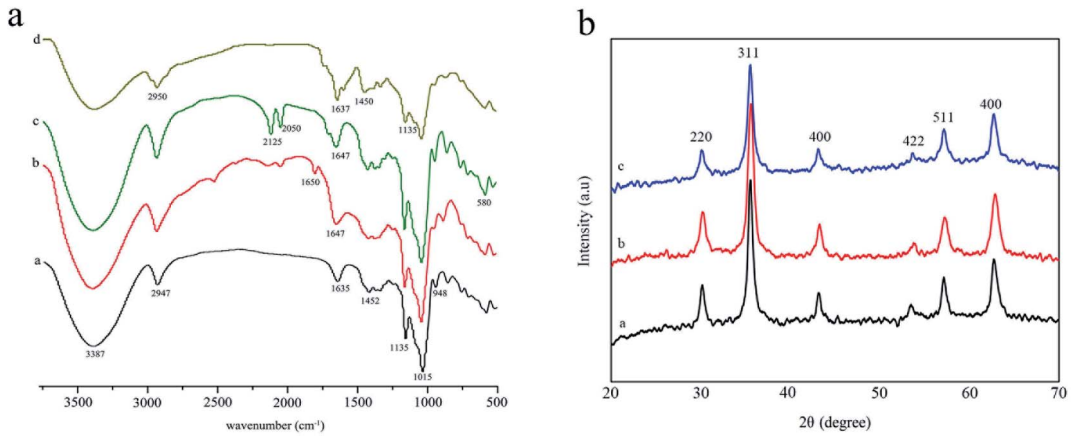

Fig. 1 Characterization of Fe_3O_4@NH_2-β-CD@GA MNPs: (a). FTIR spectra of β-CD (a), 6-NH_2-β-CD (b), Fe_3O_4@NH_2-β-CD MNPs (c) and Fe_3O_4@NH_2-β-CD@GA MNPs (d) and (b). The XRD of Fe_3O_4 MNPs (a), Fe_3O_4@NH_2-β-CD MNPs (b) and Fe_3O_4@NH_2-β-CD@GA MNPs (c).

conformed to the glucoside bond (C–O–C) anti-symmetric vibrations and coupled vibrations (C–C/C–O) of GA, which suggested that GA was loaded onto the Fe_3O_4@NH_2-β-CD MNPs. All the changes indicated that the preparation of Fe_3O_4@NH_2-β-CD@GA was successful.

Fig. 1b shows the XRD spectral analysis of the products Fe_3O_4 MNPs, Fe_3O_4@NH_2-β-CD MNPs, and Fe_3O_4@NH_2-β-CD@GA MNPs. Fig. 1b-a show the XRD pattern of the Fe_3O_4 MNPs. Compared with the standard XRD pattern of Fe_3O_4 (JCPDS file 79-0417, magnetite), the observed reflections at 30.1°, 35.4°, 43.1°, 56.9°, 62.8° were identified.[32] For Fe_3O_4@NH_2-β-CD@GA MNPs, the observed reflections at (30.2°, 220), (35.5°, 311), (43.2°, 400), (53.7°, 422), (57.2°, 511), and (62.7°, 440) were identified. For Fe_3O_4 MNPs (Fig. 1b-b) and Fe_3O_4@NH_2-β-CD@GA MNPs (Fig. 1b-c), the characteristic peaks of Fe_3O_4 MNPs were always present. The results indicated that the modification did not change the crystal structure of the Fe_3O_4 MNPs and the Fe_3O_4@NH_2-β-CD@GA MNPs were successfully prepared.

The crystallographic structures of the Fe_3O_4@NH_2-β-CD@GA MNPs and Fe_3O_4@NH_2-β-CD@GA MNPs were analyzed using HRTEM (Fig. 2). The images in Fig. 2a1 and b1 show that the Fe_3O_4@NH_2-β-CD MNPs and Fe_3O_4@NH_2-β-CD@GA MNPs have a substantially spherical-like core–shell structure, where the core is Fe_3O_4 (black region) and the shell is 6-NH_2-β-CD (gray region), confirming the direct deposition of a 6-NH_2-β-CD particle layer on the surface of Fe_3O_4 MNPs, and that no amorphous 6-NH_2-β-CD was observed. The circular streak image in Fig. 2a2 reveals the orientation of the crystalline Fe_3O_4 core, and the diameter spacing of 0.27 nm, which agrees with that of the standard magnetite of Fe_3O_4.[33] Another diameter spacing of 0.47 nm was measured in the shell layer, which could be ascribed to the amorphous Fe_3O_4 phase,[34] as shown in Fig. 2a2. The electron diffraction pattern exhibits spotty diffraction rings and well-resolved spots in Fig. 2a3, which confirm the crystalline structure of the nanoparticles.

The size distribution and zeta potential of Fe_3O_4@NH_2-β-CD MNPs and Fe_3O_4@NH_2-β-CD@GA MNPs were determined immediately after the production by using a Zetasizer instrument (Fig. 3). The average particle sizes of Fe_3O_4@NH_2-β-CD MNPs and Fe_3O_4@NH_2-β-CD@GA MNPs were 119.4 ± 0.37 nm and 147.4 ± 0.28 nm and their polydispersity indexes (PDIs) were 0.092 ± 0.025 and 0.072 ± 0.013, respectively. The zeta potentials of Fe_3O_4@NH_2-β-CD MNPs and Fe_3O_4@NH_2-β-CD@GA MNPs were −30.8 ± 0.16 mV and −29.3 ± 0.42 mV, respectively. These results show that the particle size of Fe_3O_4@NH_2-β-CD MNPs increased after loading GA. According to the report, nanoparticles with a positive surface charge are prone to interact non-specifically with serum proteins in blood and produce precipitation. The negative zeta potential of the nanoparticles suggested that they could have a prolonged circulation time in blood. The zeta potential of Fe_3O_4@NH_2-β-CD@GA MNPs was about −29.3 mV, which meant they were not dispersed stably as the electrostatic repulsion could not prevent the colloids from flocculation.

The magnetic properties of Fe_3O_4 MNPs, Fe_3O_4@NH_2-β-CD MNPs, and Fe_3O_4@NH_2-β-CD@GA MNPs were investigated by VSM (Vibrating Sample Magnetometer, NanoMagnetics Instruments) at 300 K. Their hysteresis loops could be clearly observed in Fig. 4. In the S-shape magnetic curve, no coercivity and remnant magnetization were observed, suggesting that samples were superparamagnetic.[35] Superparamagnetic materials do not retain magnetization before and after exposure to an external magnetic field, which is very useful in *in vivo* applications. The saturation magnetization values for Fe_3O_4, Fe_3O_4@NH_2-β-CD MNPs, and Fe_3O_4@NH_2-β-CD@GA MNPs were 56.86, 53.64, and 41.75 emu g^{-1}, respectively. The saturation magnetization value of Fe_3O_4@NH_2-β-CD@GA MNPs was considered to be sufficient for drug delivery. The decrease in the saturation magnetization value was attributed to the non-magnetic β-CD on the particles, quenching the magnetic moment.

As a drug-loading material, Fe_3O_4@NH_2-β-CD MNPs not only have the size effect and strong adsorption capacity of magnetic nanoparticles, but also have a hydrophobic and hydrophilic cavity inside the cyclodextrin. The GA content in the Fe_3O_4@NH_2-β-CD@GA MNPs was measured using HPLC. The

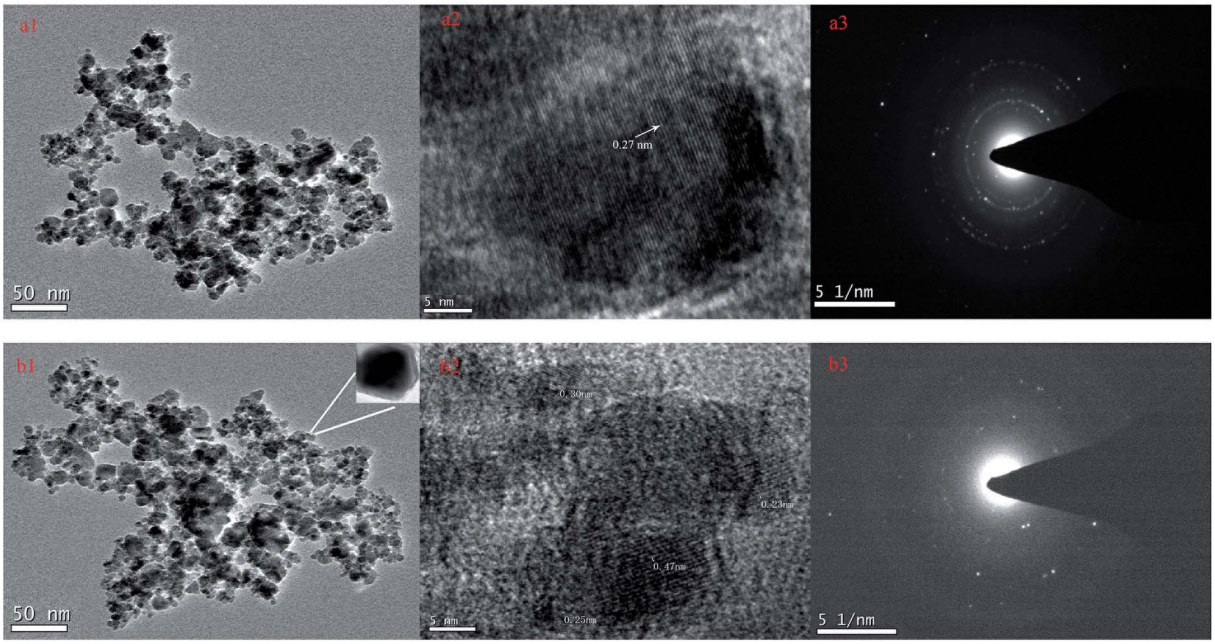

Fig. 2 The HRTEM image of Fe_3O_4@NH_2-β-CD MNPs (a1, a2, a3) and Fe_3O_4@NH_2-β-CD@GA MNPs (b1, b2, b3).

EE% and DL% of the GA in the Fe_3O_4@NH_2-β-CD@GA MNPs were 85.71 ± 3.47% and 4.63 ± 0.04%, respectively.

During the preparation of 6-NH_2-β-CD, β-CD was prone to clathration, whereas it was difficult to dissolve TosCl in water, and the whole reaction system was heterogeneous. Therefore, using water as a solvent can effectively inhibit the clathration of β-CD. When the reaction temperature exceeds 10 °C and the NaOH concentration is too high, the resulting 6-OTs-β-CD can be easily hydrolyzed. There are two main reactions for the formation of an azide group: one is Pd/C reduction, and the other is triphenylphosphine reduction. The Pd/C reduction was more intense and produces more by-products. The reduction

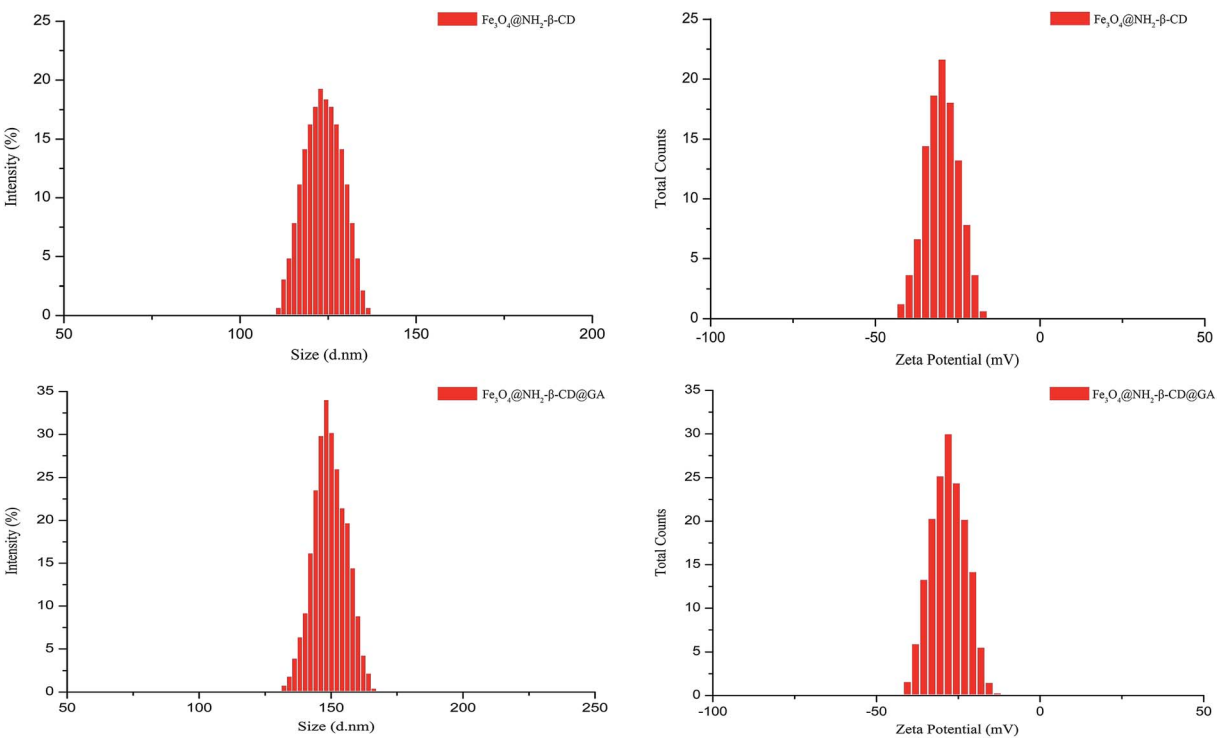

Fig. 3 The size distribution and zeta potential distribution of Fe_3O_4@NH_2-β-CD MNPs and Fe_3O_4@NH_2-β-CD@GA MNPs (n = 3).

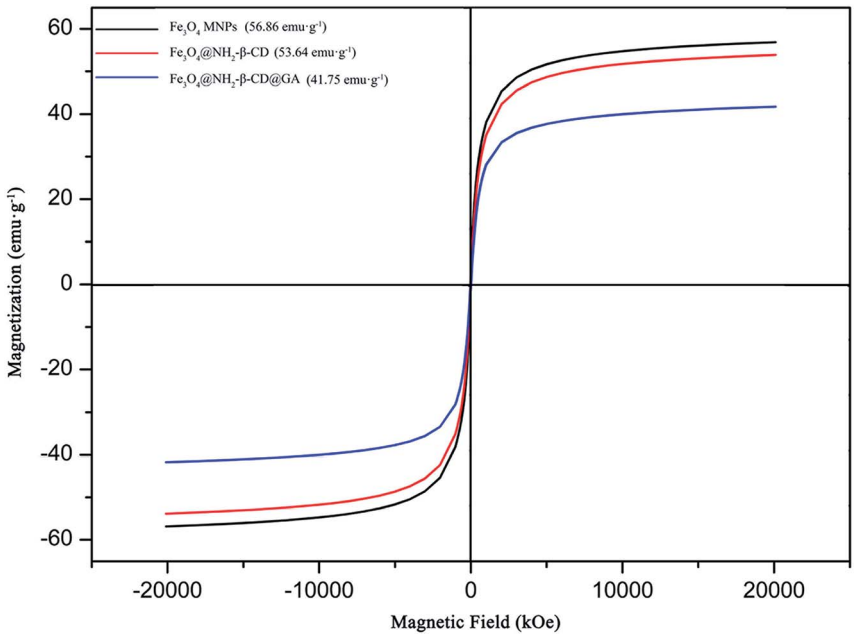

Fig. 4 The saturation magnetization curve of Fe_3O_4 MNPs, Fe_3O_4@NH_2-β-CD MNPs, and Fe_3O_4@NH_2-β-CD@GA MNPs.

reaction of triphenylphosphine was milder, and the structure of the phosphorimide could be obtained, while the use of acetone was effective for preventing the re-dissolution of triphenylphosphine in aqueous ammonia.

In the synthesis of Fe_3O_4 MNPs, stirring was carried out using polytetrafluoroethylene. Citric acid is a polycarboxyl molecule that may be adsorbed by Fe_3O_4 during the synthesis process, which can reduce the surface energy of the molecule, can effectively prevent the occurrence of agglomeration, and also act as a dispersant or electrostatic stabilizer in the synthesis process.[36] The β-CD was modified into 6-NH_2-β-CD, and its action was more inclined to provide –NH_2, which formed a chemical bond with –COOH and was grafted onto Fe_3O_4.[37] In addition, 6-NH_2-β-CD can also be used as an inclusion material, whereby the hydrophobic cavity can load a poorly soluble drug and act as a drug carrier. Fe_3O_4 has one molecule of FeO with sp^2 hybridization and one molecule of Fe_2O_3 with sp^3 hybridization, according to the principle of Pauli [exclusion] principle.[38] Fe_3O_4 can provide an empty orbital to chelate with acid ions. Furthermore, as the Fe_3O_4 forms nanoparticles, the surface energy and adsorption capacity were greatly increased, and the free acid ions were adsorbed on the surface of the Fe_3O_4 in the solution. Finally, Fe_3O_4–COOH was formed.

There are three main reasons for the decrease in saturation magnetization. First, the original spin state of the ferroferric oxide has changed. Second, with the nanocrystallization of Fe_3O_4, non-collinear rotation occurs, resulting in a decrease in the magnetic moment and magnetic properties, or rather it can be said that the surface curvature of the particle is affected by the size, and this changes the disordered crystal orientation of the particle surface, resulting in a change in saturation magnetization. Third, after Fe_3O_4 was encapsulated by NH_2-β-CD, the magnetic strength of the magnetic center was weakened.

4.2 *In vitro* drug release

The suitability of Fe_3O_4@NH_2-β-CD MNPs as drug carriers was evaluated using cumulative drug release experiments. Fig. 5 shows the release percent of GA released from Fe_3O_4@NH_2-β-CD@GA MNPs under different pH conditions. The results revealed that Fe_3O_4@NH_2-β-CD@GA MNPs showed the highest release efficiency, where the cumulative release percent was nearly 30% within 100 min under pH 7.4. The cumulative release of GA was lower at pH 4.0. However, in subsequent drug releases, the difference was not obvious under different pH conditions. As Fig. 5 indicates, the GA release from Fe_3O_4@NH_2-β-CD@GA MNPs constituted three different phases: an initial relatively fast phase, an acceleration phase, and a smooth release phase, which would help in sustaining the drug to be available for a longer period of time and helping reduce the toxic side effects of the drugs.

4.3 Cytotoxicity analysis

In an attempt to understand the anticancer efficacy of Fe_3O_4@NH_2-β-CD@GA MNPs *in vitro*, APL HL-60 and HepG2 cells, being two different cancer cell lines, were treated with different concentrations of GA, Fe_3O_4@NH_2-β-CD, and Fe_3O_4@NH_2-β-CD@GA MNPs for 24 h. The MTT assay showed that GA was able to inhibit the growth of HL-60 cells and HepG2 cells, with IC_{50} values of 0.818 μg mL^{-1} and 1.525 μg mL^{-1}, respectively. Additionally, as observed from the decrease in corresponding IC_{50} values (0.348 and 0.964 μg mL^{-1} in HL-60 and HepG2 cells, respectively) in the two cancer cell lines, after GA was encapsulated into Fe_3O_4@NH_2-β-CD, the

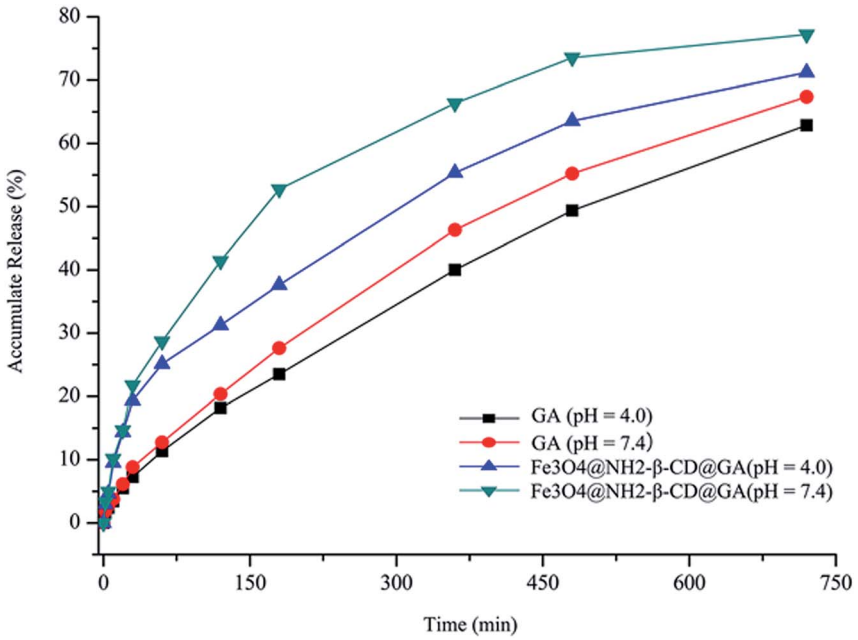

Fig. 5 Accumulative release of GA and Fe_3O_4@NH_2-β-CD@GA MNPs over time under different pH conditions ($n = 3$).

antiproliferative efficacy was greatly augmented. Furthermore, in HL-60 and HepG2 cells, Fe_3O_4@NH_2-β-CD@GA MNPs compared to GA at an equivalent drug concentration showed higher cytotoxicity, while Fe_3O_4@NH_2-β-CD demonstrated no obvious cytotoxicity, indicating its good safety with the cells, as shown in Fig. 6.

4.4 Vascular irritability

Macroscopic observations were performed for a single ear injection of GA and Fe_3O_4@NH_2-β-CD@GA MNPs to rabbits. In the GA group, significant redness, congestion, and agglomeration occurred in the injection area of the rabbit ear,[39] but no such phenomena occurred in the Fe_3O_4@NH_2-β-CD@GA MNPs group. As presented in Fig. 7d–f, there was significant swelling, degeneration, vascular edema, inflammatory cell infiltration, necrosis, and formation of thrombus when the dose of injection was increased. No pathological change was found in the control group (Fig. 7a–c). There was no degeneration, necrosis, and endothelial cell injury with the inner wall of veins, and a slight swelling in Fe_3O_4@NH_2-β-CD@GA MNP groups was observed, as shown in Fig. 7g–i. This suggested that the vascular irritation of GA could be reduced with Fe_3O_4@NH_2-β-CD MNP encapsulation due to the reduction of the direct contact of the drug with the vascular endothelium. Therefore, it could be acceptable for intravenous administration.

4.5 Pharmacokinetic characteristics

The pharmacokinetic characteristics were evaluated using i.v. administration at a single dose of 20 mg kg^{-1} of GA and Fe_3O_4@NH_2-β-CD@GA MNPs in rats, respectively. The

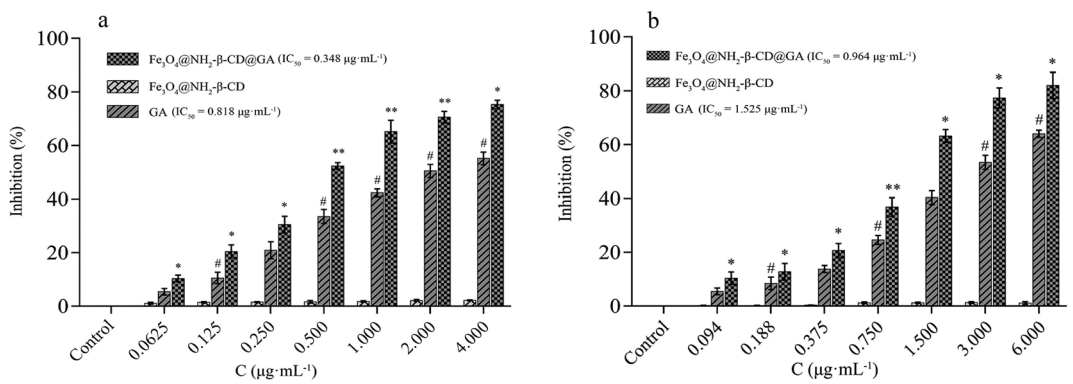

Fig. 6 Effects of GA, Fe_3O_4@NH_2-β-CD MNPs, and Fe_3O_4@NH_2-β-CD@GA MNPs on the cell viability of (a) HL-60; (b) HepG2. Cells in 96-well plates were treated with various concentrations of GA, Fe_3O_4@NH_2-β-CD MNPs, and Fe_3O_4@NH_2-β-CD@GA MNPs for 24 h (mean ± SD, $n = 3$).*$p < 0.05$, **$p < 0.01$ compared with the Fe_3O_4@NH_2-β-CD MNPs, $^{\#}p < 0.05$, $^{\#\#}p < 0.01$ compared with the GA.

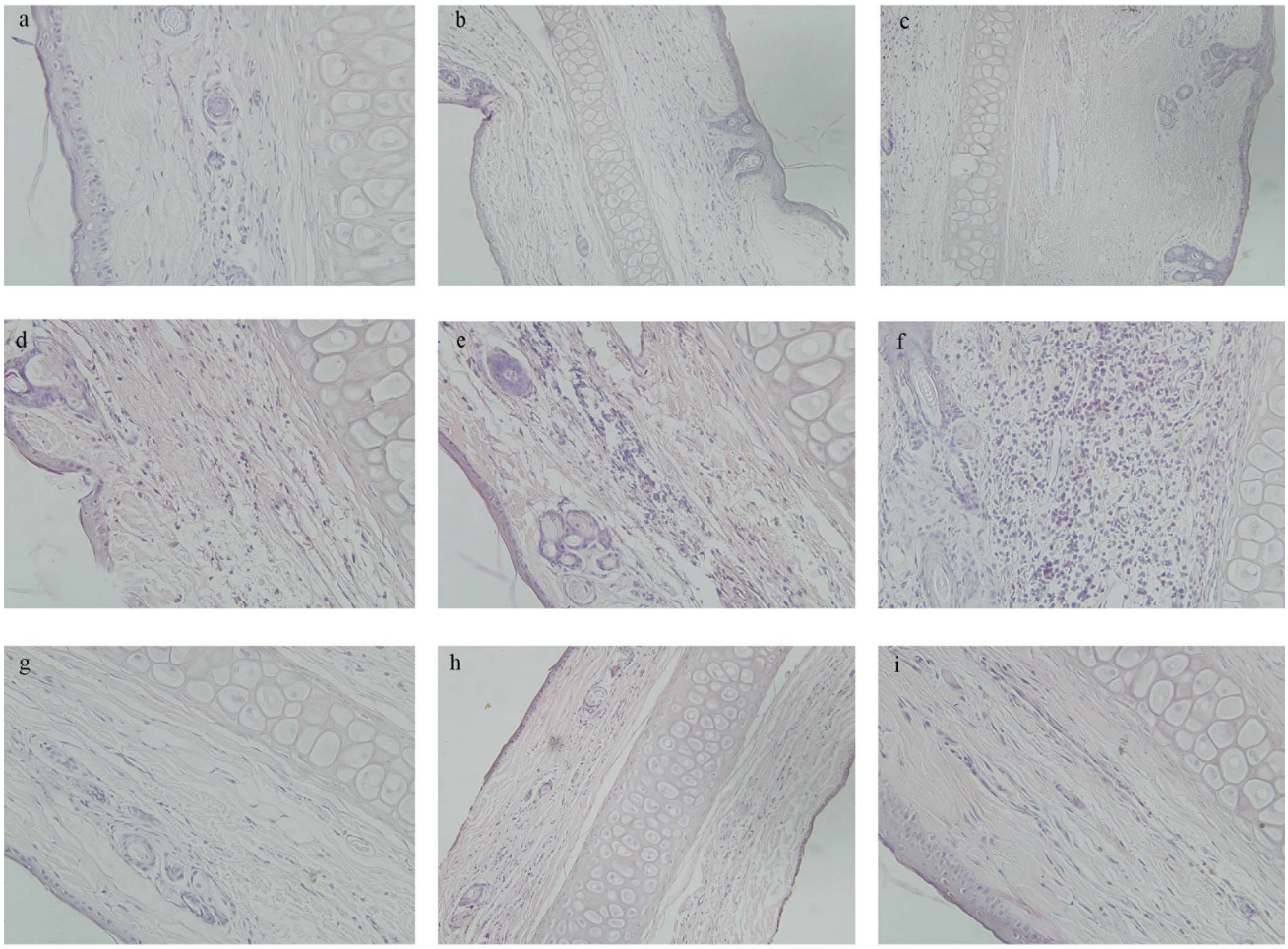

Fig. 7 Pathological paraffin sections (hematoxylin-eosin stain) from the ears of rabbits (×200 magnification). Control group (a–c), GA group (d–f), Fe_3O_4@NH_2-β-CD@GA MNPs (g–i).

pharmacokinetic parameters were calculated using DAS 2.1 software and the noncompartment model. The pharmacokinetic parameters are listed in Table 1, respectively, and the concentration-time profiles of GA and Fe_3O_4@NH_2-β-CD@GA MNPs are presented in Fig. 8. Encapsulating GA in Fe_3O_4@NH_2-β-CD greatly increased the systemic drug exposure; the AUC increased from (149.2 ± 11.91 mg (L min)$^{-1}$) to (347.8 ± 13.71 mg (L min)$^{-1}$), and the C_{max} value in the Fe_3O_4@NH_2-β-CD@GA MNPs group was significantly higher than in the GA group ($p < 0.01$). In addition, the $t_{1/2}$ value of Fe_3O_4@NH_2-β-CD@GA MNPs was significantly improved to 18.823 ± 0.409 min compared with that of the GA group. These results suggested that Fe_3O_4@NH_2-β-CD@GA MNPs could overcome the low bioavailability and poor pharmacokinetics of GA. The *in*

Table 1 Pharmacokinetic parameters of GA in plasma following administration of GA and Fe_3O_4@NH_2-β-CD@GA MNPs to rats (mean ± SD, $n = 6$)

Parameters	GA	Fe_3O_4@NH_2-β-CD@GA
$t_{1/2z}$ (min)	6.932 ± 0.392	18.823 ± 0.409[a]
C_{max} (mg L^{-1})	7.54 ± 0.56	11.82 ± 0.27[b]
CLz (L (min kg)$^{-1}$)	0.150 ± 0.004	0.062 ± 0.024[b]
$AUC_{(0-t)}$ (mg (L min)$^{-1}$)	149.2 ± 11.76	347.801 ± 13.72[b]
$AUC_{(0-\infty)}$ (mg (L min)$^{-1}$)	199.968 ± 15.36	414.707 ± 14.62[a]

[a] $p < 0.05$. [b] $p < 0.01$ compared with the GA group.

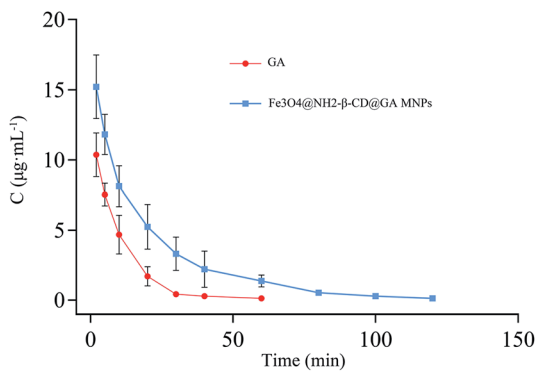

Fig. 8 Mean concentration-time profile of GA and Fe_3O_4@NH_2-β-CD@GA MNPs in plasma following i.v. administration of a single dose of 20 mg kg^{-1} to rats (mean ± SD, $n = 6$).

vivo pharmacokinetic study proved that the Fe_3O_4@NH_2-β-CD@GA MNPs exhibited slower clearance and higher drug exposure than GA did. The reason for this is that β-CD themselves have a sustained release feature, and the other reason is that the aminated modification increases this characteristic.[40] Besides, the concentration–time characteristic curve *in vivo* did not exactly match the *in vitro* release profile. The amount of released GA over 12 h was approximately 67% in the GA group, while the half-life was approximately 6.9 min after i.v. administration to the rats, which corresponded to a release amount of about 4.8% *in vitro*. The amount of released GA over 12 h was 75% in the Fe_3O_4@NH_2-β-CD@GA MNPs group *in vitro*, while the half-life was approximately 18.8 min after i.v. administration to rats *in vivo*. Some studies suggest that changes in the morphology and surface electronic structure of nanoparticles may have an effect on the pharmacokinetics *in vivo*.[41] These results provided us some information that Fe_3O_4@NH_2-β-CD themselves may have a sustained release feature to understand the properties of Fe_3O_4@NH_2-β-CD@GA MNPs with respect to pharmacokinetics and pharmacodynamics.

Fe_3O_4@NH_2-β-CD@GA MNPs possessed better magnetic targeting, controlled release, low stimulation, and good pharmacokinetic behavior *in vivo*, including a lower CLz, longer half-life, and increased AUC, which indicate that they have a good promoting effect on enhancing drug accumulation and adsorption at the tumor site when compared with gambogic acid nanomagnetic systems, such as gambogic acid-loaded micelles based on chitosan derivatives,[42] magnetic nanoparticles of Fe_3O_4 with gambogic acid,[43] GO-modified Fe_3O_4/SiO_2 nanoparticles with combined rhenium-188 and gambogic acid,[44] and gambogic acid-loaded magnetic Fe_3O_4 nanoparticles.[45] Moreover, other nanomagnetic systems, such as pegylated liposomes loaded with cisplatin magnetic nanoparticles (Cis-MLs),[46] and folic acid-functionalized magnetic nanoparticles[47] also have great significance.

5. Conclusions

Fe_3O_4@NH_2-β-CD@GA MNPs based on the host macromolecule Fe_3O_4@NH_2-β-CD and the guest component GA showed a substantially spherical-like core–shell structure with an average size of 147.4 nm and zeta potential of −29.3 mV. Besides, the Fe_3O_4@NH_2-β-CD@GA MNPs showed enhanced stability, sustained drug release profiles, and essentially increased cytotoxicity compared with free GA. Moreover, Fe_3O_4@NH_2-β-CD@GA MNPs could extend the biological half-life and improve the vascular irritability and bioavailability compared with GA. Collectively, the present results suggested that the encapsulation of GA could greatly enhance the biological activity, which also would provide more choices for Fe_3O_4@NH_2-β-CD as carriers for other hydrophobic drugs.

Conflicts of interest

There are no conflicts to declare.

Acknowledgements

The project was supported by a grant from National Natural Science Foundation of China (No. 81403318), Nature and Science Foundation of Department of Education, Anhui province in China (No. KJ2014A134), Undergraduate Training Projects for Innovation and Entrepreneurship, Anhui province in China (No. 2016150) and the Key project of Department of Scientific Technology, Anhui province in China (1604f0804030) Author. All animal procedures were performed in accordance with the Guidelines for Care and Use of Laboratory Animals of Anhui University of Chinese Medicine and experiments were approved by the Animal Ethics Committee of Anhui University of Chinese Medicine.

References

1 S. Rajput and M. Mandal, *Eur. J. Cancer Prev.*, 2012, **21**, 205–215.
2 G. M. Huang, Y. Sun, X. Ge, *et al.*, *World J. Gastroenterol.*, 2015, **21**, 6194–6205.
3 Q. Guo, Q. You, Z. Wu, *et al.*, *Acta Pharmacol. Sin.*, 2004, **25**, 769–774.
4 F. Liu, X. Huang, L. Han, M. Sang, L. Hu, B. Liu, B. Duan, P. Jiang, X. Wang, Z. Qiao, C. Ma, W. Liu, J. Liu, F. Feng and W. Qu, *Biomater. Sci.*, 2019, **7**, 1028–1042.
5 X. Tang, J. Sun, T. Ge, K. Zhang, Q. Gui, S. Zhang and W. Chen, *Colloids Surf., B*, 2018, **172**, 26–36.
6 S. Zhang, Q. Li, L. Zhang, H. Sun and Q. You, *Chin. J. Org. Chem.*, 2012, **32**, 1450–1458.
7 B. Andrzejewski, W. Bednarski, M. Kaźmierczak, *et al.*, *Composites, Part B*, 2014, **64**, 147–154.
8 Q. A. Pankhurst, J. Connolly, S. K. Jones, *et al.*, *J. Phys. D: Appl. Phys.*, 2003, **36**, R167–R181.
9 O. Veiseh, J. W. Gunn and M. Zhang, *Adv. Drug Delivery Rev.*, 2010, **62**, 284–304.
10 C. Sun, J. Lee and M. Zhang, *Adv. Drug Delivery Rev.*, 2008, **60**, 1252–1265.
11 H. Mittal, V. Parashar, S. B. Mishra and A. K. Mishra, *Chem. Eng. J.*, 2014, **255**, 471–482.
12 J. L. Gong, B. Wang, G. M. Zeng, C. P. Yang, C. G. Niu, Q. Y. Niu, W. J. Zhou and Y. Liang, *J. Hazard. Mater.*, 2009, **164**, 1517–1522.
13 R. A. Frimpong and J. Z. Hilt, *Nanomedicine*, 2010, **5**, 1401–1414.
14 V. D. M. Frank, T. Vermonden, C. F. Van Nostrum, *et al.*, *Biomacromolecules*, 2009, **10**, 3157–3175.
15 T. Loftsson and D. Duchene, *Int. J. Pharm.*, 2007, **329**, 1–11.
16 R. Holm, C. Schönbeck, P. Somprasirt, P. Westh and H. Mu, *J. Inclusion Phenom. Macrocyclic Chem.*, 2014, **80**, 243–251.
17 C. E. Jensen, R. A. dos Santos, A. M. Denadai, C. F. Santos, A. N. Braga and R. D. Sinisterra, *Molecules*, 2010, **15**, 4067–4084.
18 L. Huang, H. Wang, B. Li, E. Li, Y. Zhou, Y. Yang, C. Dong and S. Shuang, *J. Inclusion Phenom. Macrocyclic Chem.*, 2014, **80**, 209–215.

19 P. Huang, L. L. Yang, C. Y. Wang, J. P. Chen, S. S. Wang, S. J. Wang, Y. J. Chen, D. L. Wang and H. P. Huang, *J. Nanosci. Nanotechnol.*, 2015, **15**, 4774–4783.
20 H. Li, M. H. El-Dakdouki, D. C. Zhu, G. S. Abela and X. Huang, *Chem. Commun.*, 2012, **48**, 3385–3387.
21 I. A. Anan'Eva, E. N. Myshak, E. N. Shapovalova, *et al.*, *J. Anal. Chem.*, 2003, **58**, 461–466.
22 S. A. Kulkarni, P. S. Sawadh, K. K. Kokate, *et al.*, *Foundation of Computer Science (FCS)*, 2012.
23 M. Filippa, M. I. Sancho and E. Gasull, *J. Pharm. Biomed. Anal.*, 2008, **48**, 969–973.
24 Z. Tao, Y. Zhou, J. Lu, W. Duan, X. He, L. Lin, J. Ding and Y. Qin, *Cancer Biol. Ther.*, 2014, **6**, 691–696.
25 R. Mu, N. Lu, J. Wang, Y. Yin, Y. Ding, X. Zhang, H. Gui, Q. Sun, H. Duan, L. Zhang, Y. Zhang, X. Ke and Q. Guo, *Eur. J. Cancer Prev.*, 2010, **19**, 61–67.
26 N. Lu, Y. Yang, Q.-D. You, Y. Ling, Y. Gao, H.-Y. Gu, L. Zhao, X.-T. Wang and Q.-L. Guo, *Cancer Lett.*, 2007, **258**, 80–89.
27 K. Hao, X.-P. Zhao, X.-Q. Liu and G.-J. Wang, *Biomed. Chromatogr.*, 2007, **21**, 279–283.
28 S. Kaamyabi, D. Habibi and M. M. Amini, *Bioorg. Med. Chem. Lett.*, 2016, **26**, 2349–2354.
29 T. Loftsson and M. Masson, *Int. J. Pharm.*, 2001, **225**, 15–30.
30 E. Sikorska, M. Dawgul, K. Greber, E. Ilowska, A. Pogorzelska and W. Kamysz, *Biochim. Biophys. Acta*, 2014, **1838**, 2625–2634.
31 G. Trettenhahn and A. Köberl, *Electrochim. Acta*, 2007, **52**, 2716–2722.
32 A. Taufiq, Sunaryono, E. G. Rachman Putra, *et al.*, *Mater. Sci. Forum*, 2015, **827**, 213–218.
33 E. Liu, H. Yuan, Z. Kou, X. Wu, Q. Xu, Y. Zhai, Y. Sui, B. You, J. Du and H. Zhai, *Sci. Rep.*, 2015, **5**, 11164–11173.
34 Z. C. Xu, Y. L. Hou and S. H. Sun, *J. Am. Chem. Soc.*, 2007, **129**, 8698–8699.
35 H. Ebrahimzadeh, E. Moazzen, M. M. Amini and O. Sadeghi, *Anal. Methods*, 2012, **4**, 3232–3237.
36 M. Namvari and H. Namazi, *Polym. Int.*, 2014, **63**, 1881–1888.
37 L. Fan, C. Luo, M. Sun, H. Qiu and X. Li, *Colloids Surf., B*, 2013, **103**, 601–607.
38 F. Tennie, V. Vedral and C. Schilling, *Phys. Rev. A*, 2017, **95**, 022336–022345.
39 R. Li, Y. Chen, F. Zhao, Y. Liu, L. Wen and L.-l. Zeng, *Chin. J. Oncol.*, 2009, **31**, 810–814.
40 S. S. Banerjee and D.-H. Chen, *J. Nanopart. Res.*, 2008, **11**, 2071–2078.
41 M. Hadjidemetriou, Z. Al-Ahmadi, M. Mazza, *et al.*, *ACS Nano*, 2015, **9**, 8142–8156.
42 X. Zhu, C. Zhang, X. Wu, *et al.*, *Drug Dev. Ind. Pharm.*, 2008, **34**, 2–9.
43 B. Chen, Y. Liang, W. Wu, J. Cheng, *et al.*, *Int. J. Nanomed.*, 2009, **4**, 251–259.
44 Y. Yang, Y. Liu, C. Cheng, *et al.*, *ACS Appl. Mater. Interfaces*, 2017, **9**, 28195–28208.
45 C. Wang, H. Zhang, Y. Chen and B. Chen, *Int. J. Nanomed.*, 2012, **7**, 781–787.
46 A. Toro-Cordova, M. Flores-Cruz, J. Santoyo-Salazar, *et al.*, *Molecules*, 2018, **23**, 2272–2288.
47 K. Niemirowicz, H. Car, A. Sadowska, *et al.*, *J. Biomed. Nanotechnol.*, 2017, **13**, 665–677.